Aerosol and Air Quality Research, 12: 583–591, 2012

ISSN: 1680-8584 print / 2071-1409 online
doi: 10.4209/aaqr.2012.01.0015

Removal of Gaseous Ammonia in Pt-Rh Binary Catalytic Oxidation

Chang-Mao Hung[1*], Wen-Liang Lai[2], Jane-Li Lin[2]

[1] *Department of Vehicle Engineering, Yung-Ta Institute of Technology and Commerce, 316 Chung-Shan Road, Linlo, Pingtung 909, Taiwan*
[2] *Department of Environmental Science and Occupational Safety and Hygiene, Tajen University, 20 Wei-Shin Road, Yanpu Shiang, Pingtung 907, Taiwan*

ABSTRACT

In this study, the oxidation of ammonia (NH_3) to form nitrogen was investigated by selective catalytic oxidation (SCO) over a Pt-Rh binary catalyst fabricated by the incipient wetness impregnation process in a tubular fixed-bed flow quartz reactor (TFBR). The catalysts were analysed by three-dimensional excitation-emission fluorescent matrix (EEFM) spectroscopy, UV-Vis absorption, dynamic light-scattering (DLS), zeta potential measurements, and linear sweep voltammograms (LSV). At optimum conditions, namely, a temperature of 673 K and an oxygen content of 4%, nearly 100% of the NH_3 was removed by catalytic oxidation over the Pt-Rh binary catalyst. The main product of the NH_3-SCO process was N_2. Additionally, for the freshly prepared Pt-Rh binary catalyst, three peaks (at 235/295 nm, 245/315 nm, and 240/365 nm) were observed via EEFM; however, the peak with the highest emission wavelength disappeared over time as Pt-Rh binary catalyst was exhausted by NH_3. These results show that EEFM spectroscopy, which enhances intrinsic emission Pt clusters in the Pt-Rh binary catalyst, is an effective method for characterizing this catalyst in catalytic treatment systems. The UV-Vis absorption spectra revealed that the bands associated with such octahedral platinum (IV) species were observed at about 350 nm. Moreover, the LSV reversible redox ability may explain the significant activity of the catalysts.

Keywords: Selective catalytic oxidation (SCO); Tubular fixed-bed reactor (TFBR); Ammonia (NH_3); Pt-Rh binary catalyst; Excitation-emission fluorescent matrix (EEFM).

INTRODUCTION

Presently, the emission of ammonia (NH_3) is a well environmental problem involving the atmospheric formation of acidic aerosols when NH_3 reacts with HNO_3 to produce NH_4NO_3 species (Lin *et al.*, 2005; Lemmetty *et al.*, 2007; Lin *et al.*, 2008; Lin *et al.*, 2009; Han *et al.*, 2011; Li *et al.*, 2011; Oh *et al.*, 2011; Peng *et al.*, 2011). NH_3 is emitted by a number of various processes, including urea manufacturing, nitrogen fertilizer production, biomass and coal gasification, petroleum refining and refrigeration, livestock waste, and animal agriculture (Chen *et al.*, 2003; Heish *et al.*, 2010; Calvo *et al.*, 2011; Osada *et al.*, 2011). Ammonia is a corrosive, highly toxic and reactive inorganic gas with a pungent odour under ambient conditions that potentially presents a public health and environmental concern (Galloway *et al.*, 2008; Meng *et al.*, 2010; Puckett *et al.*, 2011; Hung, 2011a). Hence, the removal of NH_3 from air and waste streams and the control of NH_3 emissions are important global issues. In recent years, several approaches have been developed as a remediation processes to biologically, physically and chemically treat NH_3, such as biological nitrification, air-stripping, scrubbing with water, post-combustion control, adsorption by activated carbon and so on. However, each of these approaches causes a phase transformation and may yield contaminated sludge or adsorbent, which must be further treated because of strict discharge level requirements.

The most promising and widely used technology for solving NH_3 pollution is the selective catalytic oxidation (SCO) of ammonia (SCO-NH_3) to produce N_2 and H_2O (Hung, 2006; Hung, 2008a; Cui *et al.*, 2010; Hung, 2010; Hung, 2011b). This important heterogeneous catalytic process has attracted significant attention in materials chemistry and the effectiveness of the oxidation process has been improved by using high-performance catalysts, which potentially shorten the reaction time of the oxidation and allow the reaction to proceed under milder operating conditions. Usually, the SCO-NH_3 process selectively produces nitrogen and prevents further oxidation of nitrogen. Various kinds of catalysts that oxidize gaseous NH_3 have been examined. For example, de Boer *et al.* (1993) studied

* Corresponding author. Tel.: +886-8-7233733 ext. 508; Fax: +886-8-7228046
E-mail address: hungcm1031@gmail.com

the selective conversion of NH_3 to N_2 over V_2O_5, MoO_3, and WO_3 catalysts on various supports at 525 K in the SCO reaction. Amblard *et al.* (2000) performed excellent selective conversion of NH_3 to gaseous nitrogen using a γ-Al_2O_3-supported Ni catalyst in an SCO process. It was found that the activation of surface NH_x to be the rate limiting step. Schmidt-Szałowski *et al.* (1998) proposed a hypothetical mechanism of the effect of these catalysts, their activity and their selectivity in oxidizing NH_3. Wang *et al.* (1999) investigated the use of Ni-based catalysts for oxidizing the fuel gas that is produced by the gasification of biomass. This study revealed that fresh Ni-based catalysts were more active at lower temperatures in the decomposition of NH_3 and that the partial pressure of hydrogen in the flue gas determined the extent of NH_3 oxidation. Liang *et al.* (2000) examined the oxidation of NH_3 in a fixed-bed micro-reactor over a temperature range of 873 to 1023 K at a GHSV of 1800 to 3600/hr and found that the conversion of NH_3 reached 98.7% and 99.8% on nitrided MoNx/α-Al_2O_3 and NiMoNy/α-Al_2O_3 catalysts, respectively. Additionally, a recent study described the efficient catalytic oxidation of NH_3 in a gaseous stream using a nanoscale copper-cerium bimetallic catalyst in a temperature range of 423 to 673 K at a GHSV of 92,000/hr. The bimetallic nanoscale structure had the greatest NH_3 reduction activity, and the N_2 selectivity exhibited a synergistic effect (Hung, 2008b). Brüggemann and co-workers (2009) stated that a density functional theory of the effect of H-ZSM5 catalysts and their activity and selectivity in oxidizing NH_3. Zhang *et al.* (2009) demonstrated the excellent selective conversion of NH_3 to N_2 over a Ag-Al_2O_3 catalyst at 413 K in a SCO process. Weststrate *et al.* (2010) tested the surface chemistry of Ir(111) by radiation for NH_3 oxidation in a temperature range of 400 to 500 K. It was found that the activation of surface NH_{ad} to be the most stable species during which N_{ad}, N_2, NH_3 and some H_2 are formed.

Platinum-based metal additives can be used as three-way catalysts (TWC), and due to their selective catalytic properties, they are the most active components in hydrocarbon oxidation and are active in methanol fuel cell electro-oxidation reactions, as reported elsewhere (Anderson, 1993; Choi *et al.*, 2004). The use of rhodium-based metal improves the nitrogen oxide conversion properties of the catalysts, including selectivity towards dinitrogen and reduces poisoning by carbon monoxide (Stoyanovskii *et al.*, 2009). Normal operating conditions are well within the ranges of stability of platinum and rhodium and of the components that are used to stabilize the surface area of the catalyst (Zhang and Geddes, 2010). More important, few studies have investigated the use of the Pt-Rh binary material in the catalytic gaseous-phase oxidation of NH_3. Accordingly, this paper concerns the activity of the Pt-Rh binary catalyst in the oxidation of NH_3 under various conditions and the effect of this catalyst on the decomposition of NH_3 in SCO processes.

However, EEFM data on the fluorescence emission of most of these catalysts are available from their detailed chemical and physical characterization. Studies of fluorescence emission, especially of platinum-based composite materials, which have been used for decades, are available, but very little is known about the fluorescence of most of the newly developed materials and their interaction with metal structures. Herein, excitation-emission fluorescence matrix (EEFM) spectroscopy was used as an effective tool across a range of excitation and emission wavelengths to understand information regarding catalyst characteristics during catalytic process. Moreover, the catalysts were measured by UV-Vis absorption, dynamic light-scattering (DLS), zeta potential, and linear sweep voltammograms (LSV).

MATERIALS AND METHODS

Materials and Chemicals

The Pt-Rh binary catalysts used in this work were prepared by the incipient wetness impregnation method with aqueous H_2PtCl_6 and $Rh(NO_3)_3$ (all grade, Merck, Darmstadt, Germany). The precipitate was washed with distilled water before being dried at 473 K for 10 hours. The Pt-Rh binary catalyst, which had a Pt to Rh weight ratio of 3 to 1, was wash-coated on a γ-Al_2O_3 substrate with a constant active metals ratio of 3%. The catalysts were then calcined at 673 K in an air stream for 4 hours. The resulting powder was formed into tablets using acetic acid as a binder. The tablets were sequentially reheated at 573 K to burn off the binder and then crushed. Finally, various particle sizes ranged from 0.25 to 0.15 mm was completed using a different meshes of screen.

Experimental Methods

The experiments were conducted in a tubular fixed-bed quartz reactor (TFBR). The typical reactant gas was composed of 800 ppm NH_3, 4% O_2, and He and flowed into the inlet of the reactor (GHSV, 92,000/hr). A mass flow regulator was used to independently control the flows of NH_3 and O_2. Highly pure He was used as a carrier gas at a flow rate ranging from 8 to 13 L/min and was controlled using a mass flow meter (830 Series Side-Trak^{TM}, Sierra, Monterey, CA, USA). This approach resembled that of Hung (2008b), who conducted experiments on the catalytic oxidation of NH_3. A reaction tube with a length of 300 mm and an inner diameter of 28 mm was placed inside a split tube furnace with the tube that contained the catalyst. The temperature was measured using two type-K thermocouples (KT-110, Kirter, Kaohsiung, Taiwan), each with a diameter of 0.5 mm, located in front of and behind the catalytic bed. The thermocouples were also connected to a PID controller (FP21, Shimaaen, Tokyo, Japan) to maintain the temperature in the tube within ±0.5%.

Instrumental Analyses

Before and after the reaction, the samples were automatically injected through a sampling valve into a gas chromatograph (Shimadzu GC-14A), equipped with a thermal conductivity detector. A stainless-steel column (Porapak Q 80/100 mesh) was used to separate the components of the gas and determine the concentration of the product (N_2O and N_2) that was formed. The areas associated with the signals were electronically measured using a data integrator (CR-6A, Shimadzu, Kyoto, Japan). Dilute sulfuric acid was

used to scrub the residual NH_3 in the vapour gas, and the amount of NH_3 was measured using a Merck kit (Merck, Spectroquant Pharo 300, Darmstadt, Germany). The concentrations of NO, NO_2 and O_2 in the gas samples were monitored continuously during the reaction at a particular location in the reactor, using a portable flue gas analyser (IMR-3000, Neckarsulm, Germany). Data were collected after the SCO reaction had reached steady-state, which was typically after 20 min at each temperature. Each temperature was maintained for 90 min to allow the system to reach steady-state. Most experiments were repeated once to ensure reproducibility, and similar results were always obtained.

Fluorescence excitation-emission matrix (FEEM) spectroscopy can be adopted to provide a complete spectral characterization of catalyst material. In this work, fluorescent EEM spectra were obtained using a luminescence spectrophotometer (F-4500, Hitachi, Japan) with a xenon lamp as the excitation source. The emission spectra are plotted on the x-axis while the excitation spectra are potted parallel to the y-axis. The widths of all slits at both the excitation and emission monochromators were 10 nm. In this investigation, EEFM comprised 60 excitation and 60 emission spectra from 200 to 800 nm, yielding discrete values of fluorescence intensity at 3600 excitation/emission wavelength pairs. Spectral subtraction was performed to remove the blank spectra from pure water. The UV-Vis absorption spectra of the solid samples were obtained using a photo spectrophotometer (U-2900, Hitachi, Japan). A zeta potential analyser (Zetasizer 2000HAS, Malvern, UK) was used to perform the particle size and the zeta potential determination. Linear sweep voltammograms (LSV) measurements were conducted at room temperature with an electrochemical analyser (CHI 6081D, USA) using a three-electrode electrochemical cell to investigate the oxidation/reduction of the powder samples. The working electrode (WE) was a glassy carbon electrode, and the samples were scanned at a rate of 20 mV/s with the potential cycled between –0.2 and 1.2 V. The counter electrode (CE) was a platinum wire, and a saturated hydrogen electrode (SHE) was employed as the reference electrode (RE). The electrolyte solution was H_2SO_4 (0.5 M).

RESULTS AND DISCUSSION

The experimental results presented in Fig. 1 reveal that the NH_3-SCO method is an effective method for catalysing NH_3. The overall selectivity of N_2 production was 7–56%, and that of NO production was 0–19% over the range of 15–100% NH_3 conversion at NH_3 concentrations of 800 ppm (Fig. 1). Hu *et al.* (1998) showed that nitrogen gas was formed primarily by the direct dissociation of the NO produced by oxidation of the adsorbed NH_3. Therefore, we hypothesize that NH_3 and oxygen were adsorbed onto specific sites on the Pt-Rh binary catalyst, promoting rapid conversion of NH_3 to nitrogen gas and water. Moreover, the Pt-Rh binary likely play an important role in the catalytic oxidation of ammonia, and the alumina may only offer active sites for the reaction during a catalysed oxidation run. Furthermore, catalytic activity may be caused by a strong interaction between the Pt-Rh binary and alumina. Kondarides *et al*. (1998) showed that Rh_2O_3 is the most active phase in the catalytic reaction because it is a good promoter of oxygen storage and has selectivity towards dinitrogen. However, some noble metals, such as Rh, have been used as catalysts in this catalytic process (Mulukutla *et al*., 2002). Apparently, the rhodium dioxide in a platinum catalyst has the ability to promote the formation of the active phase of PtO_2 upon the oxidation of NH_3. This catalytic analytical result is similar to that as described by Curtin *et al.* (2000). These results indicate that when gaseous oxygen

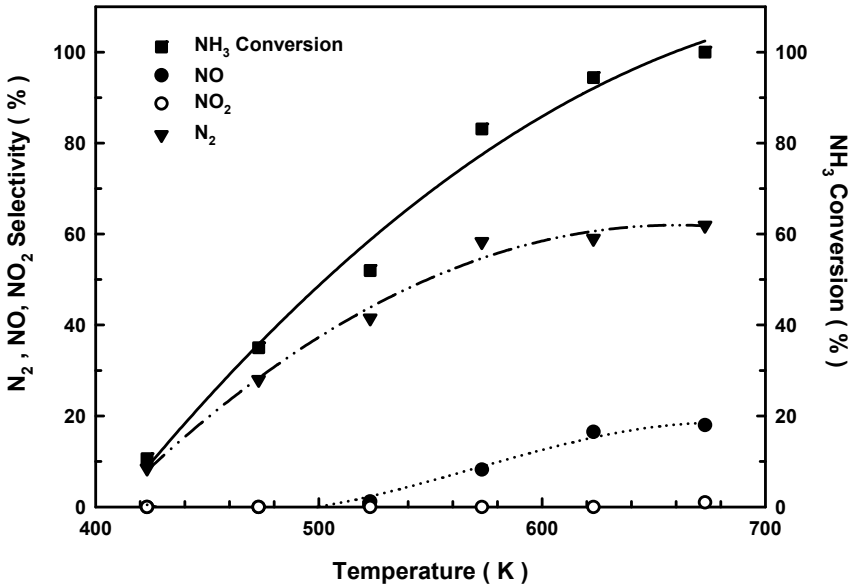

Fig. 1. The variations of the ammonia conversion, and species of N_2, NO and NO_2 yield at various temperatures over the Pt-Rh binary catalyst. Test conditions: 800 ppm NH_3 in He, O_2 = 4%, R.H. = 12%, Temp. = 423–673 K, GHSV = 92000 mL/h-g.

is fed into the reactor with NH_3, the oxidation of NH_3 becomes an unimportant step in the reaction. The oxidation of NH_3 to N_2 may be the first step in the interaction of NH_3 with excess oxygen. The availability of oxygen on the surface lattice is normally considered an essential property of oxide catalysts for selective oxidation (Curtin *et al.*, 2000). Therefore, the NH_3-SCO reaction mechanism should be selective toward nitrogen and prevent its further oxidation. Hence, this study indicates that the SCO-NH_3 process was suitable for the catalytic oxidation of NH_3.

To further elucidate the reactive property of catalyst in this work, EEFM (excitation-emission fluorescence matrix) produced from a fluorescent spectrometer can provide information about the preliminary properties of catalyst. Fig. 2(a) displays the EEFM for fresh Pt-Rh binary catalyst and has three peak locations (Ex/Em) at 235/295 nm, 245/315 nm, and 240/365 nm. Fig. 2(b) displays the EEFM of the Pt-Rh binary catalyst after an activity test and has two significant peak locations at 250/315 nm and 225/290 nm. These excitation/emission spectra of the catalyst can be explained as the metal-enhanced fluorescence (MEF) effect associated with the Pt clusters of the Pt-Rh binary catalyst surface sites during the reaction (Zhang *et al.*, 2011).

Regarding the chemical properties of the Pt-Rh binary catalyst, UV-Vis absorption spectra can provide further information of light absorbance by platinum and rhodium species. The results shown in Fig. 3 reveal that the peak band associated with such octahedral platinum (IV) species was observed at 350 nm (Fig. 3(a)), and the UV-Vis absorbance of the octahedral platinum (IV) species after the activity test show a low value at 350 nm (Fig. 3(b)). In previous work, the band at 350 nm was shown to correspond to platinum (IV) species *d-d* transitions (Bradley *et al.*, 1995; de Resende *et al.*, 1999). No rhodium-containing species are detected by UV-Vis spectroscopy. These results indicate that rhodium may exist in a highly dispersed form.

Particle size and zeta potential are important physical properties for catalyst materials research (Xu, 2008). Dynamic light-scattering (DLS) was used to assess the particle size change in the catalyst as shown in Fig. 4. The mean particle size converged to approximately 614 nm for fresh Pt-Rh binary catalyst. However, the particle size of

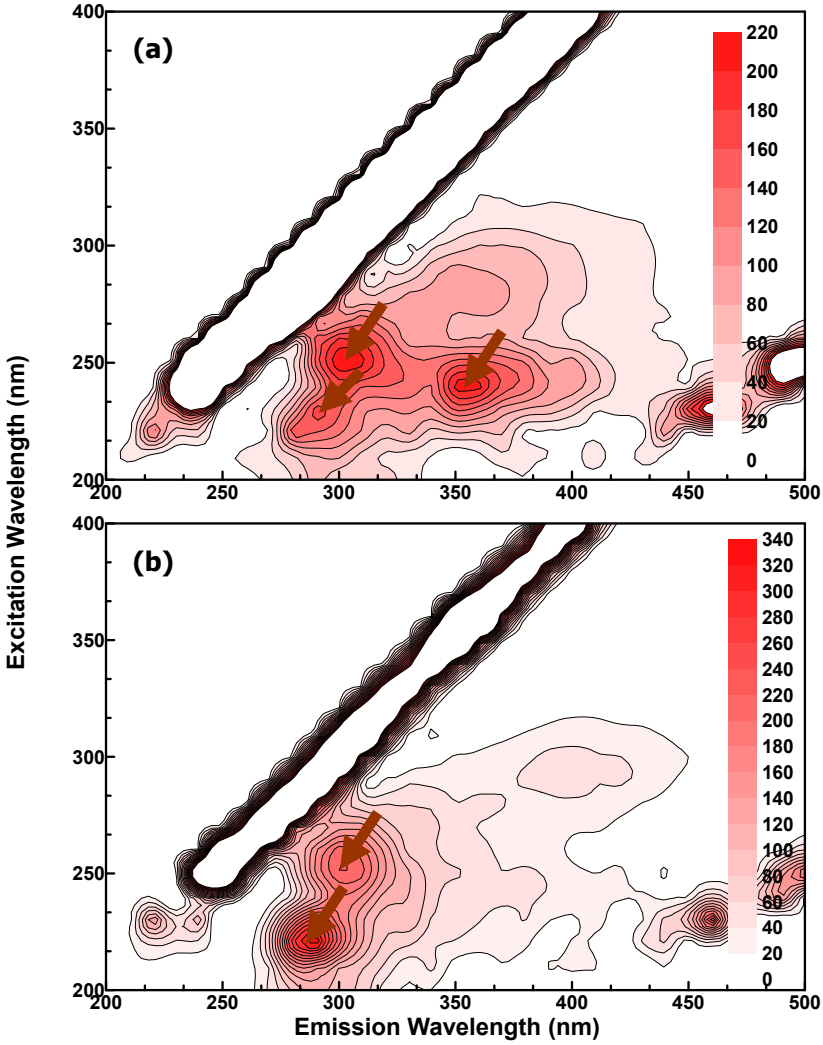

Fig. 2. The excitation-emission fluorescent matrix contour plots of (a) freshly prepared and (b) spend Pt-Rh binary after catalyst activity. Test conditions: 800 ppm NH_3 in He, O_2 = 4%, GHSV = 92000/hr.

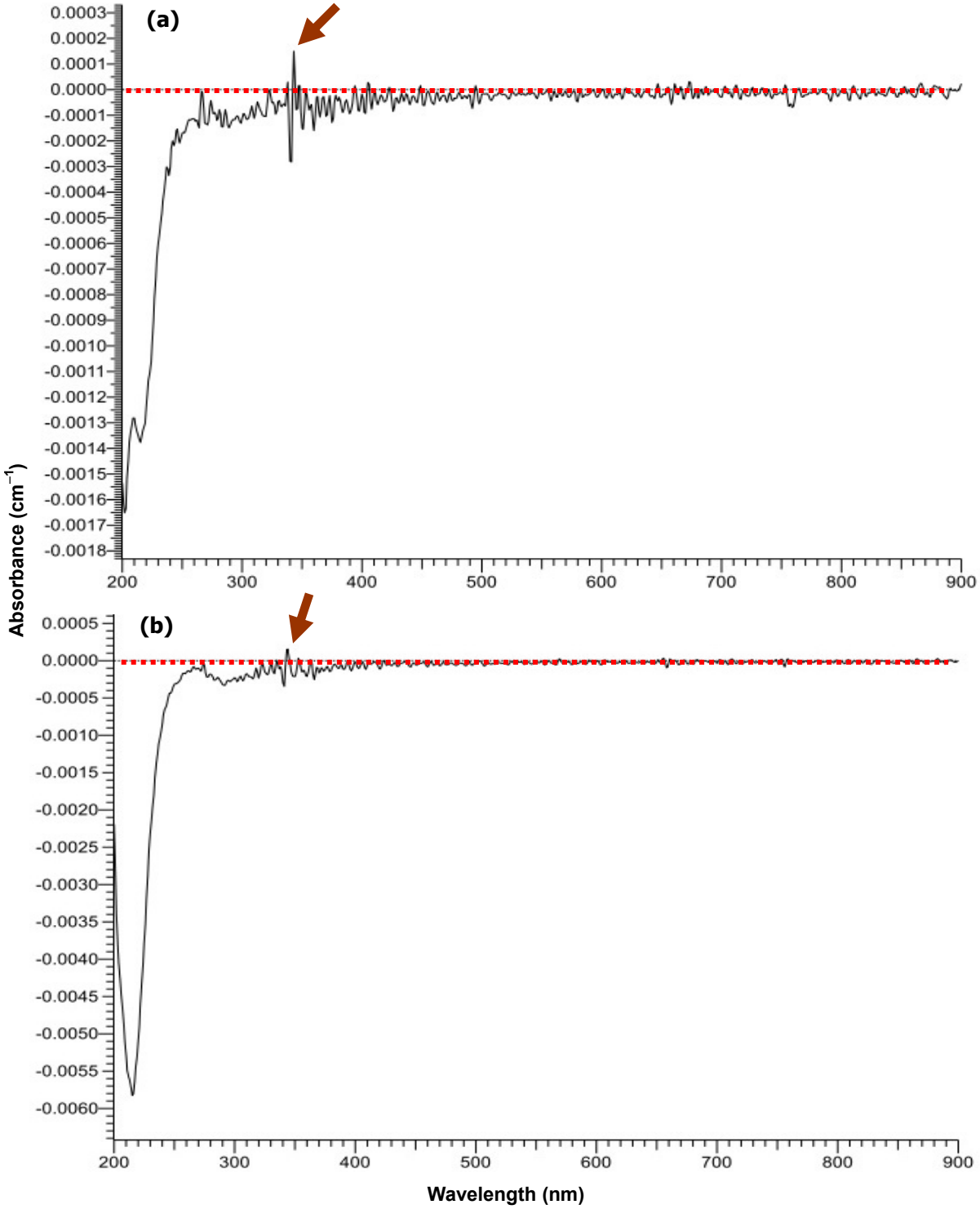

Fig. 3. UV-Vis absorption spectra of the Pt-Rh binary catalyst (a) freshly prepared and (b) spent after the activity test. Test conditions: 800 ppm NH_3 in He, O_2 = 4%, RH = 12%, GHSV = 92000/hr.

the catalyst after an activity test decreased to about 609 nm, indicating that particle migration, sintering, and coalescence may be factors that are present after the catalytic reaction (Prasad and Chavdhari, 1994). The size distribution of the Pt-Rh particles appears to be narrow. Hence, such changes in the sizes of the catalyst particles may be attributed to the over-oxidation of the Pt-Rh binary catalyst surface sites during the reaction. Fig. 5 displays the variation of zeta potentials between the freshly prepared and completely used catalysts. This variation demonstrates that the surface charge of the catalyst changes during exposure to the catalytic oxidation environment. The mean particle zeta potential changed from –18 mV for freshly prepared Pt-Rh binary catalyst to 16 mV for completely reacted Pt-Rh binary

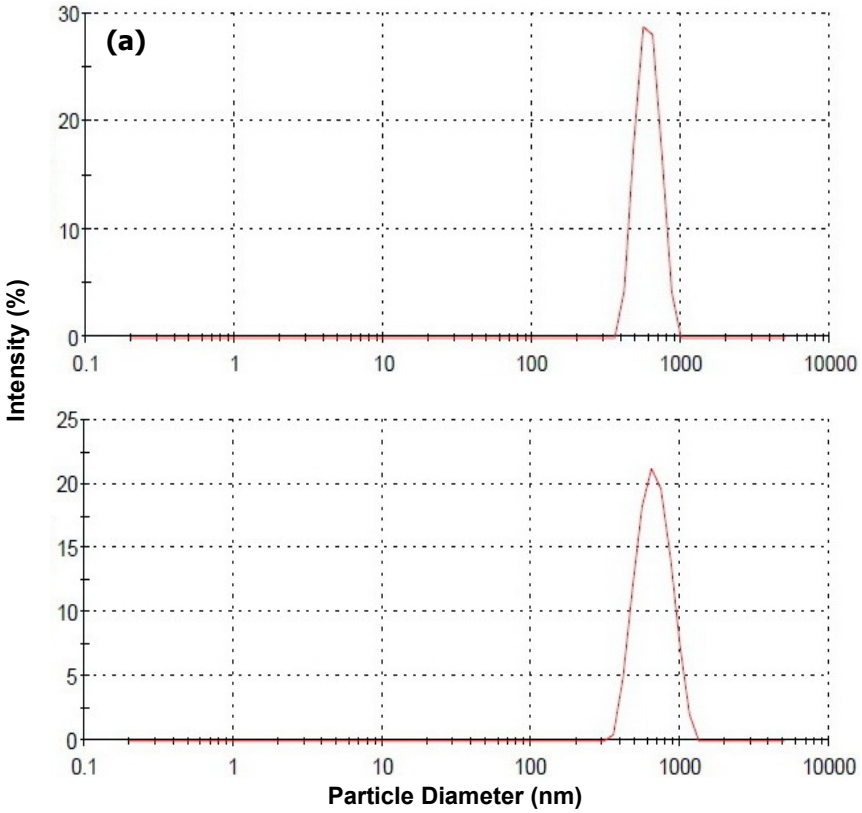

Fig. 4. Variation of the particle size distributions between the Pt-Rh binary catalyst when (a) freshly prepared and (b) completely reacted after the activity test. Test conditions: 800 ppm NH_3 in He, O_2 = 4%, GHSV = 92,000/hr.

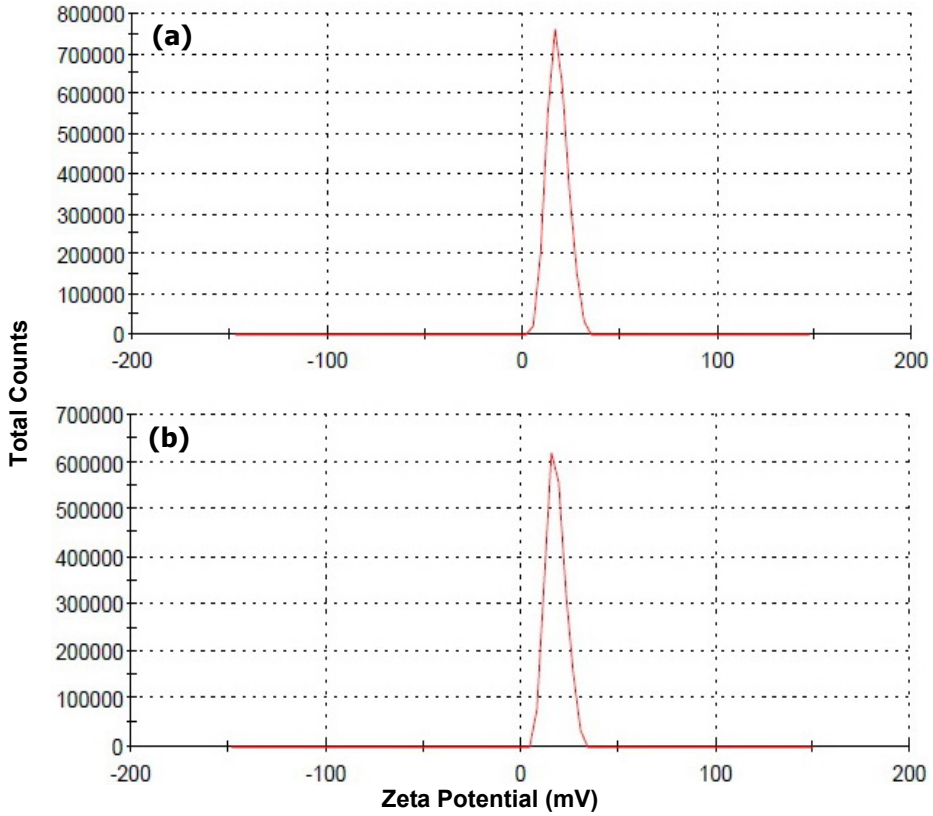

Fig. 5. Variation of the zeta potential between the Pt-Rh binary catalyst when (a) freshly prepared and (b) completely reacted after the activity test. Test conditions: 800 ppm NH_3 in He, O_2 = 4%, GHSV = 92,000/hr.

catalyst. The weak electrostatic repulsion of the solid particle surface charge and the tendency of the particles to flocculate after catalytic reaction, as shown by Du *et al.* (2008), might be significant causes explaining the phenomena that occurred in this experiment. Obviously, this explanation is consistent with the previous observation of the catalyst particle size (Fig. 4). The zeta potential that may be depend on the pH value of this platinum-based composite material, and this potential will be studied in the future.

This work also shows the electrochemical behavior of LSV profiles of the freshly prepared and aged Pt-Rh binary catalyst. A rapid rise in current density did not appear until about 0.8 V (Fig. 6). Moreover, the LSV plots reveal that the freshly prepared Pt-Rh binary catalyst has a greater reversible redox capacity and oxidation current density than the aged Pt-Rh binary catalyst, with the well-marked state at 0.5 and 0.2 V for the freshly prepared Pt-Rh binary catalyst and the aged Pt-Rh binary catalyst, respectively. This reversible redox ability explains the significant activity of the catalysts. In contrast, the aged Pt-Rh binary catalyst produces negligible oxidation-reduction current in this potential window. Prasad and Chavdhari (1994) demonstrated that Rh_2O_3 has the most active phase in the catalytic reaction owing to its strong promoter of oxygen storage. When it is present in a platinum catalyst, Rh_2O_3 has an ability to promote the formation of the active phase of PtO during NH_3 oxidation. Concerning the catalytic activity of the Pt-Rh binary catalyst system in the oxidation of NH_3, the storage and release of O_2 by the oxygen buffers because the Rh^{3+}–Rh^0 redox couple produces oxygen vacancies and increasing oxygen mobility could promote the bifunctional mechanism of the catalyst. Furthermore, the generation of rhodium hydroxide species ($Rh(OH)_x$) was evidenced by reduction peaks at 0.5 V (Oliveira *et al.*, 2008). Therefore, NH_3 is believed to be adsorbed on the surface of the catalyst before undergoing an oxidation–reduction reaction on the platinum and rhodium oxide active sites.

CONCLUSIONS

The Pt-Rh binary was selected as a highly efficient catalyst material for the SCO-NH_3 reaction to form nitrogen and was found to be as effective as other treatment methods. The overall selectivity of the NO by-product varied from 0 to 19%, and the N_2 production varied from 7 to 56% with a 15 to 100% NH_3 conversion when a Pt-Rh binary catalyst was used. The experimental results indicate that the SCO-NH_3 process is reasonably selective for nitrogen and may prevent its further oxidation. Additionally, according to a fluorescent spectrometry evaluation, fresh Pt-Rh binary catalyst yielded fluorescent plots at 235/295 nm, 245/315 nm, and 240/365 nm at room temperature. EEFM is a non-destructive and sensitive technique for developing modality for the fluorescent species detection of catalyst complexes. The particle size and zeta potential of the catalyst were determined in the catalytic process. An electrochemical characterization was performed, and the LSV over a wide potential range revealed that the reversibility of the redox may explain the significant activity of the catalysts. Thus, the Pt-Rh binary catalyst performs remarkably well in the treatment of highly concentrated streams of NH_3 in the SCO-NH_3 process and the catalyst will therefore be an efficient and practical route in industrial plants to meet increasingly stringent regulations concerning NH_3 discharge and address environmental sustainability in the future.

ACKNOWLEDGMENTS

The author would like to thank the National Science Council of the Republic of China, Taiwan, for financial support of this research under Contract No. NSC 98-2221-E-132-003-MY3.

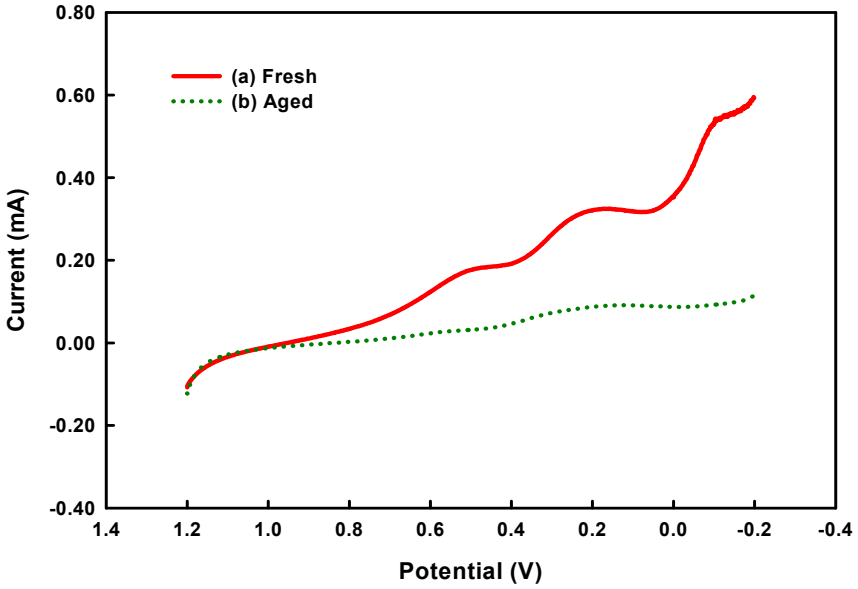

Fig. 6. Linear sweep voltammograms of the Pt-Rh binary catalyst (a) freshly prepared and (b) completely reacted after the activity test in a 0.5 M H_2SO_4 electrolyte solution recorded at a scan rate of 20 mV/s.

REFERENCES

Amblard, M., Burch, R. and Southward, B.W.L. (2000). A Study of the Mechanism of Selective Conversion of Ammonia to Nitrogen on Ni/γ-Al_2O_3 under Strongly Oxidizing Conditions. *Catal. Today* 59: 365–371.

Anderson, J.A. (1993). Infrared Study of CO Oxidation over Pt-Rh/Al_2O_3 Catalysts. *J. Catal.* 142: 153–165.

Bradley, J.M., Hopkinson, A. and King, D.A. (1995). Control of a Biphasic Surface Reaction by Oxygen Coverage: The Catalytic Oxidation of Ammonia over Pt{100}. *J. Phys. Chem.* 99: 17032–17042.

Brüggemann, T.C. and Keil, F.J. (2009). Theoretical Investigation of the Mechanism of the Selective Catalytic Oxidation of Ammonia on H-form Zeolites. *J. Phys. Chem. C* 113: 13860–13876.

Calvo, A.I., Castro, A., Pont, V., Cuetos, M.J., Sánchez, M.E. and Fraile, R. (2011). Aerosol Size Distribution and Gaseous Products from the Oven-controlled Combustion of Straw Materials. *Aerosol Air Qual. Res.* 11: 616–629.

Chen, S.J., Hsieh, L.T., Hwang, W.I., Xu, H.C. and Kao, J.H. (2003). Abatement of Odor Emissions from Landfills Using Natural Effective Microorganism Enzyme. *Aerosol Air Qual. Res.* 13: 87–99.

Choi, J.H., Park, K.W., Park, I.S., Nam, W.H. and Sung, Y.E. (2004). Methanol Electro-Oxidation and Direct Methanol Fuel Cell Using Pt/Rh and Pt/Ru/Rh Alloy Catalysts. *Electrochim. Acta* 50: 787–790.

Cui, X., Zhou, J., Ye, Z., Chen, H., Li, L., Ruan, M. and Shi, J. (2010). Selective Catalytic Oxidation of Ammonia to Nitrogen over Mesoporous CuO/RuO_2 Synthesized by Co-Nanocasting-Replication Method. *J. Catal.* 270: 310–317.

Curtin, T., Regan, F.O., Deconinck, C., Knűttle, N. and Hodnett, B.K. (2000). The Catalytic Oxidation of Ammonia: Influence of Water and Sulfur on Selectivity to Nitrogen over Promoted Copper Oxide/Alumina Catalysts. *Catal. Today* 55: 189–195.

de Boer, M., Huisman, H.M., Mos, R.J.M., Leliveld, R.G., van Dillen, A.J. and Geus, J.W. (1993). Selective Oxidation of Ammonia to Nitrogen over SiO_2-Supported MoO_3 Catalysts. *Catal. Today* 17: 189–200.

de Resende, N.S., Eon, J.G. and Schmal, M. (1999). Pt-TiO_2-γ-Al_2O_3 Catalyst I. Dispersion of Platinum on Alumina-Grafted Titanium Oxide. *J. Catal.* 183: 6–13.

Du, H.Y., Wang, C.H., Hsu, H.C., Chang, S.T., Chen, U.S., Yen, S.C., Chen, L.C., Shih, H.C. and Chen, K.H. (2008). Controlled Platinum Nanoparticles Uniformly Dispersed on Nitrogen-Doped Carbon Nanotubes for Methanol Oxidation. *Diamond Relat. Mater.* 17: 535–541.

Galloway, J.N., Townsend, A.R., Erisman, J.W., Bekunda, M., Cai, Z., Freney, J.R., Martinelli, L.A., Seitzinger, S.P. and Sutton, M.A. (2008). Transformation of the Nitrogen Cycle: Recent Trends, Questions, and Potential Solutions. *Science* 320: 889–892.

Han, S., Bian, H., Feng, Y., Liu, A., Li, X., Zeng, F. and Zhang, X. (2011). Analysis of the Relationship between O_3, NO and NO_2 in Tianjin, China. *Aerosol Air Qual. Res.* 11: 128–139.

Heish, L.T. and Chen, T.C. (2010). Characteristics of Ambient Ammonia Levels Measured in Three Different Industrial Parks in Southern Taiwan. *Aerosol Air Qual. Res.* 10: 596–608.

Hu, Z., Allen, F.M., Wan, C.Z., Heck, R.M., Steger, J.J., Lakis, R.E. and Lyman, C.E. (1998). Performance and Structure of Pt-Rh Three-Way Catalysts: Mechanism for Pt/Rh Synergism. *J. Catal.* 174: 13–21.

Hung, C.M. (2006). Selective Catalytic Oxidation of Ammonia to Nitrogen on CuO-CeO_2 Bimetallic Oxide Catalysts. *Aerosol Air Qual. Res.* 6: 150–169.

Hung, C.M. (2008a). Catalytic Decomposition of Ammonia over Bimetallic CuO/CeO_2 Nanoparticle Catalyst. *Aerosol Air Qual. Res.* 8: 489–499.

Hung, C.M. (2008b). Decomposition Kinetics of Ammonia in Gaseous Stream by a Nanoscale Copper-Cerium Bimetallic Catalyst. *J. Hazard. Mater.* 150: 53–61.

Hung, C.M. (2010). Honeycomb Cordierite-Carriers Pt-Pd-Rh Ternary Composite for Ammonia Removal. *Aerosol Air Qual. Res.* 10: 119–124.

Hung, C.M. (2011a). Fabrication, Characterization, and Evaluation of the Cytotoxicity of Platinum-Rhodium Nanocomposite Materials for Use in Ammonia Treatment. *Powder Technol.* 209: 29–34.

Hung, C.M. (2011b). Preparation, Properties and Cytotoxicity Assessment of Nanosized Pt-Rh Composite Catalyst for the Decomposition of Gaseous Ammonia. *Adv. Mat. Res.* 160–162: 1285–1290.

Kondarides, D.I., Zhang, Z. and Verykios, X.E. (1998). Chlorine-induced Alterations in Oxidation State and CO Chemisorptive Properties of CeO_2-Supported Rh Catalysts. *J. Catal.* 176: 536–544.

Lemmetty, M., Vehkamäki, H., Virtanen, A., Kulmala, M. and Keskinen, J. (2007) Homogeneous Ternary H_2SO_4–NH_3–H_2O Nucleation and Diesel Exhaust: A Classical Approach. *Aerosol Air Qual. Res.* 10: 119–124.

Li, H.C., Chen, K.S., Lai, C.H. and Wang, H.K. (2011). Measurements of Gaseous Pollutant Concentrations in the Hsuehshan Traffic Tunnel of Northern Taiwan. *Aerosol Air Qual. Res.* 11: 776–782.

Liang, C., Li, W., Wei, Z., Xin, Q. and Li, C. (2000). Catalytic Decomposition of Ammonia over Nitrided MoNx/α-Al_2O_3 and NiMoNy/α-Al_2O_3 Catalysts. *Ind. Eng. Chem. Res.* 39: 3694–3697.

Lin, C.C., Chen, S.J., Huang, K.L., Hwang, W.I., Chang-Chien, G.P. and Lin, W.Y. (2005). Characteristics of Metals in Nano/Ultrafine/Fine/Coarse Particles Collected beside a Heavily Trafficked Road. *Environ. Sci. Technol.* 39: 8113–8122.

Lin, C.C., Chen, S.J., Huang, K.L., Lee, W.J., Lin, W.Y., Tsai, J.H. and Chaung, H.C. (2008). PAHs, PAH-induced Carcinogenic Potency, and Particle-extract-induced Cytotoxicity of Traffic-related Nano/ultrafine Particles. *Environ. Sci. Technol.* 42: 4229–4235.

Lin, C.C., Huang, K.L., Chen, S.J., Liu, S.C., Tsai, J.H., Lin, Y.C. and Lin, W.Y. (2009). NH_4^+, NO_3^-, and SO_4^{2-} in Roadside and Rural Size-resolved Particles and Transformation of NO_2/SO_2 to Nanoparticle-bound NO_3^-/SO_4^{2-}. *Atmos. Environ.* 43: 2731–2736.

Meng, Z.Y., Xu, X.B., Wang, T., Zhang, X.Y., Yu, X.L., Wang, S.F., Lin, W.L., Chen, Y.Z., Jiang, Y.A. and An, X.Q. (2010). Ambient Sulfur Dioxide, Nitrogen Dioxide, and Ammonia at Ten Background and Rural Sites in China during 2007-2008. *Atmos. Environ.* 44: 2625–2631.

Mulukutla, R.S., Shido, T., Asakuru, K., Kogure, T. and Iwasawa, Y. (2002). Characterization of Rhodium Oxide Nanoparticles in MCM-41 and Their Catalytic Performances for NO-CO Reactions in Excess O_2. *Appl. Catal., A* 228: 305–314.

Oh, M.S., Lee, T.J. and Kim, D.S. (2011). Quantitative Source Apportionment of Size-segregated Particulate Matter at Urbanized Local Site in Korea. *Aerosol Air Qual. Res.* 11: 247–264.

Oliveira, R.T.S., Santos, M.C., Nascente, P.A.P., Bulhões, L.O.S. and Pereira, E.C. (2008). Nanogravimetric and Voltammetric Studies of a Pt-Rh Alloy Surface and Its Behavior for Methanol Oxidation. *Int. J. Electrochem. Sci.* 3: 970–979.

Osada, K., Ueda, S., Egashira, T., Takami, A. and Kaneyasu, N. (2011). Measurements of Gaseous NH_3 and Particulate NH_4^+ in the Atmosphere by Fluorescent Detection after Continuous Air–water Droplet Sampling. *Aerosol Air Qual. Res.* 11: 170–178.

Peng, Y.P., Chen, K.S., Wang, H.K. and Lai, C.H. (2011). In Situ Measurements of Hydrogen Peroxide, Nitric Acid and Reactive Nitrogen to Assess the Ozone Sensitivity in Pingtung County, Taiwan. *Aerosol Air Qual. Res.* 11: 59–69.

Prasad, K.V. and Chavdhari, R.V. (1994). Activity and Selectivity of Supported Rh Catalysts for Oxidative Carbonylation of Aniline. *J. Catal.* 145: 204–215.

Puckett, L.J., Tesoriero, A.J. and Dubrovsky, N.M. (2011). Nitrogen Contamination of Surficial Aquifers-A Growing Legacy. *Environ. Sci. Technol.* 45: 839–844.

Schmidt-Szałowski, K., Krawczyk, K. and Petryk, J. (1998). The Properties of Cobalt Oxide Catalyst for Ammonia Oxidation. *Appl. Catal., A* 175: 147–157.

Stoyanovskii, V.O., Vedyagin, A.A., Aleshina, G.I., Volodin, A.M. and Noskov, A.S. (2009). Characterization of Rh/Al_2O_3 Catalysts after Calcination at High Temperatures under Oxidizing Conditions by Luminescence Spectroscopy and Catalytic Hydrogenolysis. *Appl. Catal., B* 90: 141–146.

Wang, W., Padban, N., Ye, Z., Andersson, A. and Bjerle, I. (1999). Kinetic of Ammonia Decomposition in Hot Gas Cleaning. *Ind. Eng. Chem. Res.* 38: 4175–4182.

Weststrate, C.J., Bakker, J.W., Gluhoi, A.C., Ludwig, W. and Nieuwenhuys, B.E. (2010). Ammonia Oxidation on Ir(111): Why Ir is more Selective to N_2 than Pt. *Catal. Today* 154: 46–52.

Xu, R. (2008). Progress in Nanoparticles Characterization: Sizing and Zeta potential Measurement. *Particuology* 6: 112–115.

Zhang, L. and He, H. (2009). Mechanism of Selective Catalytic Oxidation of Ammonia to Nitrogen over Ag/Al_2O_3. *J. Catal.* 268: 18–25.

Zhang, S. and Zhao, Y. (2011). Facile Preparation of Organic Nanoparticles by Interfacial Cross-linking of Reversed Micelles and Template Synthesis of Subnanometer Au-Pt Nanoparticles. *Nano* 5: 2637–2646.

Zhang, Y. and Geddes, C.D. (2010). Metal-Enhanced Fluorescence from Thermally Stable Rhodium Nanodeposits. *J. Mater. Chem.* 20: 8600–8606.

Received for review, January 18, 2012
Accepted, April 5, 2012